2023 IEEE/RSJ International Conference on Intelligent Robots and Systems (IROS)
October 1-5, 2023. Detroit, USA

Motor Unit Action Potential Based Classification of Hand and Arm Motions

Michael D. Twardowski, *Member, IEEE*, Michael D. Chan, Zhi Li, Gianluca De Luca, Joshua C. Kline, and John P. Chiodini*[1]

Abstract—While motion classification architectures have improved in accuracy and robustness in recent years, computationally expensive approaches and sophisticated hardware dependencies limit their real-world applicability. To overcome these challenges, we have designed a lightweight, real-time architecture for classifying motions of the arm & hand using features derived from motor unit action potentials within surface Electromyographic (sEMG) signals, rather than which provide direct interrogation of underlying muscle activation patterns. We tested the architecture on 6 motions performed dynamically across a range of muscle contraction intensities achieving median classification accuracies ranging from 91.3% to 93.3% and an average processing time of approximately 40 ms across three different classifiers. Taken together, our findings demonstrate potential robustness of motor unit based neural interfaces for motion classification tasks.

I. Introduction

In 1993, the seminal work by Hudgins et al. [1] demonstrated that a simple linear discriminant analysis (LDA) classifier could distinguish arm motions from a given muscle in multiple degrees of freedom using features extracted from the raw signal of an electromyographic (EMG) sensor. This development laid the foundation for many of the pattern recognition algorithms found within existing commercially available prosthetic control solutions (e.g. COAPT Complete Control [2], IBT Sense [3], and Ottobock Myo Plus [4]). Subsequent improvements included the introduction of multi-sensor architectures [5], and optimization of myoelectric feature sets to maximize feature and class discriminability [6]. Despite these achievements, existing commercial myoelectric pattern recognition algorithms remain confounded by factors such as electrode position, limb orientation, and contraction intensity leading to classification accuracies < 80% [7]-[9]. Various investigations have explored mitigation strategies during classifier training to include a more representative range of muscle contraction intensities, yielding accuracies above 80 % [10]. Some works have even improved accuracies above 90% but at the expense of introducing computationally expensive offline approaches with relatively high processing times and sophisticated hardware [11], limiting their applicability. Further improvement is needed to develop accurate motion classification systems without sacrificing real-time performance. Recently, there has been growing interest in leveraging the properties of motor units – the fundamental components of sEMG signals - for motion classification tasks. The authors of [12] proposed an approach based on separation of motor unit discharge patterns, demonstrating improved accuracy over conventional amplitude-based EMG for low force levels (<25% MVC). Other technologies have advanced sEMG decomposition technology [13] to enable direct identification and tracking of motor unit action potentials (MUAPs) within the sEMG signal during dynamic movements [14], affording new opportunities to investigate motion classification leveraging features extracted from the waveforms of one or more superimposed MUAPs which constitute the sEMG signal as opposed to the raw of filtered signal. Prior work has already demonstrated that changes in muscle fiber orientation resulting from different motions alter the characteristics of MUAPs [15] observed by sEMG electrodes. These findings, coupled with the demonstrated longitudinal stability of quantitative features for tracking MUAPs throughout the sEMG signal [16], indicate that MUAPs provide a potentially data rich feature-set for interrogating and discriminating the underlying activation patterns occurring during muscle activation. In this work, we leverage our established mathematical framework evolved over decades of detecting and tracking MUAPs in both intramuscular- and surface-acquired EMG signals to develop a novel motion classification system that tracks MUAP features from multi-channel sEMG signals to achieve simultaneous real-time and high-accuracy discrimination of 3-DoF movements of the arm and hand, bridging the existing gap between motion classification accuracy and real-time performance.

II. Methods

A. Participants

A total of 10 healthy participants with no history of neuromuscular disorders volunteered for participation (5 males, 5 females; mean age 33.6 ± 16.2 yr. [range 22 - 71 yr.]). Each participant read, indicated they understood and signed informed consent forms approved by the Western

[1]Funding: The research reported in this paper was supported in part by the De Luca Foundation, Delsys Inc., and the Eunice Kennedy Shriver National Institute of Child Health and Human Development under award number R44HD094626 of the National Institutes of Health.

M. D. Twardowski was with Delsys & Altec Inc., Natick, MA 01760 USA, and with the Human Inspired Robotics Laboratory, Worcester Polytechnic Institute, Worcester, MA, 01609 USA. and is now at The MITRE Corporation, Bedford, MA 01730, USA

M. D. Chan was with Delsys & Altec Inc., Natick, MA 01760 USA and is now at Embodied, Inc.

Z. Li is with the Department of Robotics Engineering, and the Human Inspired Robotics Laboratory, Worcester Polytechnic Institute, Worcester, MA, 01609 USA

G. De Luca, JC Kline, and J. P. Chiodini are with Delsys & Altec Inc., Natick, MA 01760 USA (e-mail: jpchiodini@delsys.com).

* Corresponding author

2023 IEEE/RSJ International Conference on Intelligent Robots and Systems (IROS) | 978-1-6654-9190-7/23/$31.00 ©2023 IEEE | DOI: 10.1109/IROS55552.2023.10342444

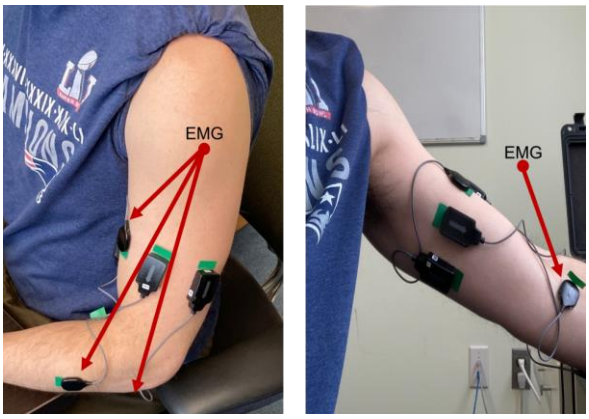

Figure1: sensors were placed over the Extensor Digitorum Communis (EDC), the Flexor Digitorum Profundus (FDP), the Pronator Teres (PT), and the Biceps Brachii (BB) muscles.

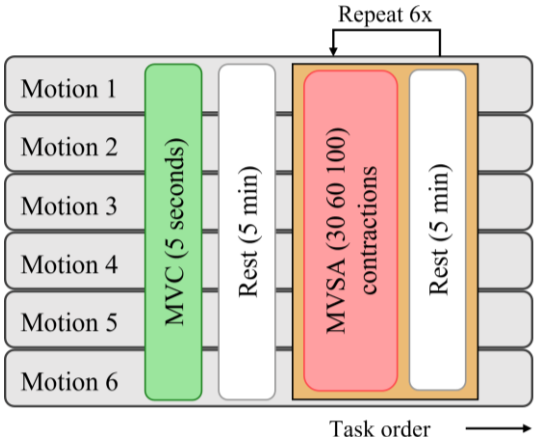

Figure 2: Experiment protocol. For each subject, we collected sets of muscle contractions comprising 6 motions. For each motion, subjects were instructed to perform an MVC contraction, followed by 6 sets of randomly chosen MVSA contractions at 30,60, and 100 percent.

Institutional Review Board (Study Number: 1154666) before participating in the study.

B. Data Acquisition

We recorded sEMG signals using 4 Trigno™ Galileo mini-grid sensors (Delsys Inc., Natick, MA) placed on the surface of the skin over the mid-belly of four muscles of the arm and forearm (Fig 1) – the Extensor Digitorum Communis (EDC), he Flexor Digitorum Profundus (FDP), the Pronator Teres (PT) and the Biceps Brachii (BB). These muscles were chosen because they represent both distally and proximally located agonists associated with one or more of the following 6 motions: 1) extension of the fingers, 2) flexion of the fingers, 3) pronation of the forearm, 4) supination of the forearm, 5) extension of the wrist, and 6) flexion of the wrist. At each sensor location, only mild skin preparation was performed by shaving excess hair with a razor, removing the superficial dead skin with medical-grade tape peels, and cleansing the skin with an alcohol swab. From each sensor, we recorded 4 differential sEMG signals, band-pass filtered them between 20 to 450 Hz, and digitized them at 2.222 kHz using a Trigno™ EMG acquisition system (Delsys Inc.). We acquired all data on a Dell Precision desktop with an Intel ® Core ™ i7-4790 CPU @ 3.60 GHz processor with 16 GB of RAM.

C. Protocol

We designed a protocol (Fig 2) to test voluntary motions of the hand and forearm in 3 degrees of freedom: 1) finger flexion/extension, 2) forearm supination/pronation and 3) wrist flexion/extension. Participants were seated with their arms unsupported with their shoulder in an anatomical resting position, and their elbow flexed 90 degrees. From this position each participant performed a Maximum Voluntary Contraction (MVC) by dynamically executing each motion individually through the full range of motion and holding it for 5 seconds. Following these recordings, each participant's Maximum Voluntary Sustained Activation (MVSA100) from the MVC was measured by 1) calculating the RMS sEMG signal of each primary muscle using a sliding 250ms window and 2) averaging the resulting RMS values from the peak activation to the end of the MVC. After an initial rest period of 5 minutes, Participants were then asked to perform 6 sets of muscle contractions. Each set was composed of contractions for each motion (18 second ramp with a 7 second hold at the plateau) at 3 intensities: from 0 to 30% (MVSA30), 60% (MVSA60) and 100% (MVSA100) of their MVSA100 while tracking an amplitude trajectory via RMS biofeedback from the agonist muscle for each respective motion, yielding 18 repetitions (6 motions, 3 intensities) per set. The order of repetitions in each set were chosen pseudorandomly. Rest periods of 5 minutes were provided between sets to avoid muscle fatigue.

D. Feature Extraction

We derived a feature set from waveforms of 1 or more superimposed MUAPs within segments of sEMG signal (Fig 3). Detected waveforms are characterized by identifying all zero crossings Z_c—defined as any location in the signal where the sign of the amplitude changes—and then splicing the signal into a set of biphasic shapes, each comprising 3 consecutive zero crossings. Each spliced waveform was composed of two phases of opposite polarity, one between the first and second zero crossings, and the other between the second and third zero crossings. From this set of shapes, we retain only those with peak amplitudes exceeding the noise baseline of the signal, and a phase amplitude ratio threshold >4:1 to separate waveforms composed of action potentials from signal noise and artifacts. Waveforms satisfying these criteria are then isolated from the surrounding signal at the zero crossing locations adjacent to their left and right phases across all 4 channels of each sensor. From these data, 5 major MUAP features were computed:

1) Positive Peak Amplitude (P_{pos})

The positive peak amplitude is defined as the maximal peak amplitude value within the positive phase of the biphasic waveform. The peak amplitude functions as an indicator of signal energy, and it is well known that the local energy of the EMG signal is directly related to the force generation within a muscle [17]. Peak amplitude measures directly interrogate

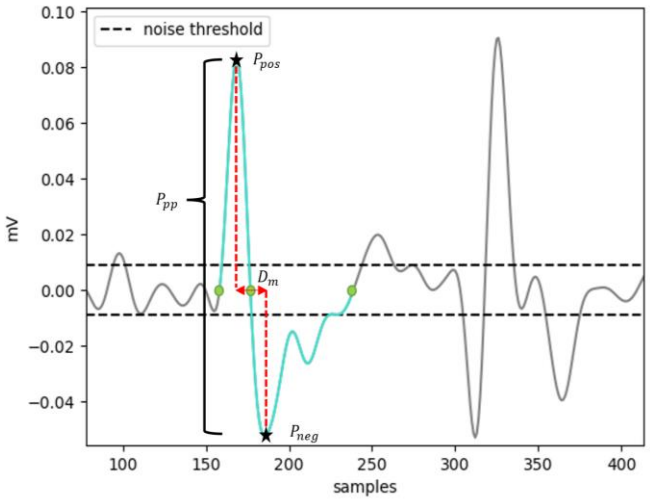

Figure 3: Visual example of isolated waveform and extracted features from one channel of sEMG data. Each waveform (highlighted in blue) is isolated around the left, right, and center zero crossings. The first phase of the waveform occurs between the left and center zero crossings, while the right phase occurs between center and right zero crossings. Amplitude (P_{pos}, P_{neg}, P_{pp}) and width (D_m) features are denoted.

the maximal energy value within the waveform while remaining invariant to the low amplitude noise which surrounds MUAPs and their superpositions.

2) Negative Peak Amplitude (P_{neg})

The negative peak amplitude is defined as the minimal peak amplitude value for the negative phase of the biphasic waveform. In addition to the properties mentioned for P_{pos}, peak amplitude can also serve as an indicator regarding the ratio of positive to negative energy within a waveform.

3) Peak to peak amplitude (P_{pp})

We have defined peak to peak amplitude as $P_{pp} = |P_{pos}| + |P_{neg}|$. This measure was chosen as an additional indicator of total waveform energy that is invariant to changes in phase ratio which inevitably occur in nonstationary EMG signals.

4) Main drop time (D_m)

The main drop distance measures the temporal distance between the most positive and most negative phase peak amplitudes in a waveform. This feature can be used as an indicator of waveform width as well as constituent MUAP widths and frequencies. This feature was chosen due to its relative invariance to noise artifacts as opposed to other waveform width measures such as overall waveform length, which may be biased by the presence of low energy artifacts that cause long signal tails to form between the base of the waveform and its zero-crossing location. Longer drop distances may also be used as an indicator of superimposed MUAP content as the superposition of multiple offset MUAPs can cause the summed waveform to increase in width.

5) Total zero crossings (ZcT)

Total zero crossings count the number of detected waveforms within a given window of data. At low values, ZcT

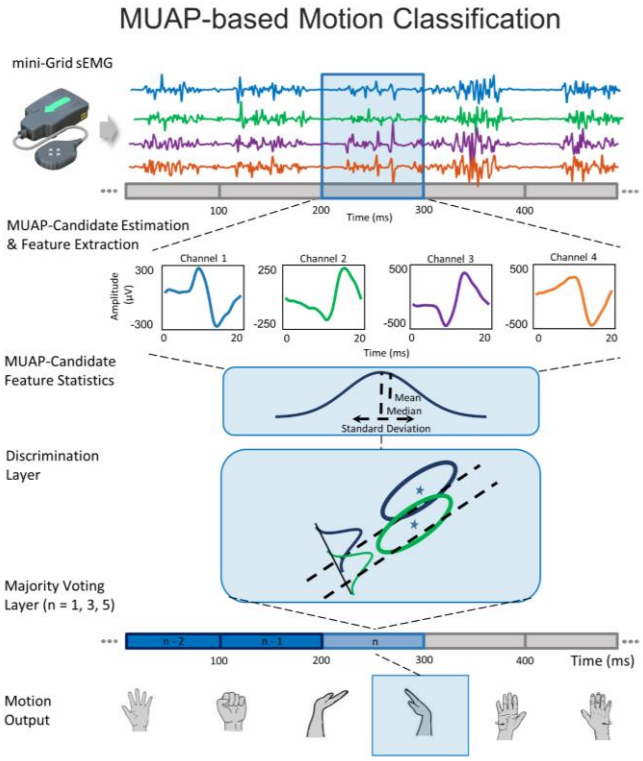

Figure 4: A schematic diagram of the MUAP-based motion classification architecture. This architecture estimates waveforms comprising MUAPs in the sEMG signal, extracts their features, and performs inference on a motion classifier to predicts their respective motion.

may be used as an indicator of signal sparsity, while at higher values may indicate the presence of larger amounts of MUAP activity.

To standardize our features across windows of data that invariably contain different numbers of waveforms, we calculated mean, standard deviation, and median for each of the 5 MUAP features across all channels and added the tally of waveforms found for a total number of 244 features for each window of sEMG data ([5 MUAP features x 3 population statistics x 4 channels + 1 isolated waveform] x 4 sensors = 244).

E. Algorithm Architecture

Our pattern recognition architecture (Fig 4) comprises two main stages: 1) A training stage in which the classifier learns to discriminate between 6 motions – finger flexion, finger extension, wrist flexion, wrist extension, forearm pronation, and forearm supination; and 2) a testing stage in which the classifier performs rapid inference on the intended motions. Both modules were implemented in Python. As an initialization stage, for each placed sensor, signals were recorded while all the participant's muscles are relaxed to estimate baseline noise and DC offset thresholds for each sEMG channel.

1) Data Pre-processing

We divided each participant's data of 108 contractions (6 motions with 6 repeated trials performed up to 3 target

TABLE I. Confusion matrix of motion classification accuracy for LDA, MLP, and SVM classifiers.

Classifier LDA (%) MLP (%) SVM (%)	Finger Flexion	Finger Extension	Wrist Flexion	Wrist Extension	Forearm Pronation	Forearm Supination
Finger Flexion	**93.7%** **92.4%** **88.3%**	0.9% 2.9% 3.4%	3.4% 2.1% 2.0%	0.7% 0.9% 0.9%	0.6% 0.2% 0.4%	0.9% 0.4% 0.7%
Finger Extension	1.4% 2.0% 4.2%	**88.3%** **85.1%** **83.4%**	0.8% 0.6% 0.4%	7.8% 8.1% 8.7%	0.9% 0.4% 0.6%	1.7% 0.6% 0.6%
Wrist Flexion	2.3% 2.8% 3.0%	0.9% 0.5% 0.8%	**93.2%** **94.2%** **94.2%**	0.3% 0.1% 0.4%	1.1% 0.7% 0.9%	2.6% 0.9% 2.0%
Wrist Extension	1.0% 1.0% 1.0%	9.3% 10.0% 11.3%	0.5% 0.3% 0.4%	**90.0%** **87.1%** **86.9%**	2.9% 1.7% 1.9%	2.3% 0.9% 1.1%
Forearm Pronation	0.6% 1.0% 2.3%	0.1% 0.6% 0.3%	0.3% 1.2% 1.3%	0.3% 2.2% 1.4%	**93.6%** **95.8%** **94.9%**	0.2% 1.1% 0.7%
Forearm Supination	1.0% 0.7% 1.2%	0.5% 0.9% 0.7%	1.9% 1.6% 1.6%	0.8% 1.6% 1.7%	1.1% 1.2% 1.4%	**92.4%** **96.1%** **94.9%**

activation levels) into training and testing sets. We randomly assigned 2 of each motion trial performed up to MVSA30 and 2 performed up to MVSA100 to a training set, with the remaining trials assigned to the testing set. This represents a 22% to 78% training to testing split (24 training contractions and 84 testing motions). Both training and test data were parsed into non-overlapping 100-ms segments.

2) Classifier Training

We trained an LDA, support vector machine (SVM) and a multi-layer perceptron (MLP) commonly used in pattern recognition applications [10] using the scikit-learn library [18]. After extracting features from each training segment, we performed standardization using scikit's *StandardScaling* method, which calculates and removes each feature's mean and scales them to unit variance. These calculated values are then stored and used to standardize the MUAP-based features from the test motions. We used the default LDA classifier, the radial-basis function kernel for the SVM classifier with probability estimation and set the maximum iterations to n=15000 and set the maximum iterations to n=15000 for the MLP with 3 hidden layers with node counts of 300, 150, and 50 and trained using back propagation to ensure training fit convergence. Once training is complete, a set of weights and parameters are stored for each classifier for use in subsequent testing stages.

3) Classifier Testing

To test each trained classifier, we designed a custom pipeline to load existing trained classifiers, sequentially load test data segments from hard disk into memory and run them through the pipeline to simulate real-time incoming sEMG data. We implemented real-time feature extraction algorithms using the Numba library [19] allowing us to utilize the multi-threading capabilities of the CPU to compute features from multiple waveforms in parallel. These algorithms process each segment in the pipeline, extracting 244 features per segment. Extracted features are passed to the classification stage, they are run through the trained classifier to obtain one of 6 possible motion output results for each segment. Our architecture made final classification decisions for each window using a voting size of n=1, i.e. classification decisions are made for each 100 ms window of data based solely on the given window's data.

TABLE II. Processing time performance for LDA, MLP, and SVM classifiers in training and testing phases

	Pipeline	Processing Time(s)	Max Real-Time Ratio
LDA	Training	89.9±6.7 (max=102.9)	
	Testing	0.039±0.018 (max=0.098)	0.98/1
MLP	Training	91.9±5.1 (max=98.1)	
	Testing	0.039±0.019 (max=.108)	1.08/1
SVM	Training	91.6±5.6 (max=99.9)	
	Testing	0.039±0.019 (max=.097)	0.97/1

III. RESULTS

A. Classification Accuracy

Confusion matrices from the predictions for each tested classifier's accuracy for majority voting n=1 across all participants are shown in Table 1. The accuracy of each motion was measured by the correctly classified 100-ms windows divided by the number of total test windows. A non-parametric Wilcoxon rank sum test was used to evaluate the differences between the accuracies for each classifier. Across all participants the MLP classifier demonstrated the highest performance with a median accuracy of 93.3% across all motions. The LDA classifier demonstrated the second highest performance with an overall median accuracy of 92.8% which was not significantly different than the performance of the MLP classifier (p=1.00). The SVM classifier demonstrated the lowest performance with a median accuracy of 91.3%, though its performance was not significantly different than that of the LDA classifier (p=0.43), or the MLP classifier (p=0.38).

B. Processing Time

The summary of the processing performance of each classifier pipeline is detailed in Table 2. The average training time for each classifier was 89.9, 91.9, and 91.6 seconds for the LDA, MLP, and SVM respectively. When testing on 100 ms windows of data, the LDA classifier demonstrated the fastest average testing times (0.037 ±0.018 s, max= 0.098 s) and a maximum real time ratio of 0.98/1. The SVM classifier demonstrated the second fastest average testing times (0.039 ±0.019 s, max= 0.097 s) and a maximum real time ratio of 0.97/1. Finally, the MLP classifier demonstrated the slowest average testing times (0.039 ±0.019 s, max= 0.108 s) and a maximum real time ratio of 1.08/1.

IV. Discussion

Our MUAP-based motion classifier performed real-time capable classification of 6 targeted motions from 4 sEMG sensors, achieving median accuracies ranging from 91.3% to 93.3%. To test motion viability, we collected dynamic contractions which varied in force and kinematic joint angle of hand and arm at a variety of contraction intensities. Our classifiers operate on n=1 nonoverlapping voting windows of 100ms suitable for classification of both shorter and longer duration dynamic contractions, achieving average processing times < 40ms per window in all classifiers. Future work will expand our testing to encompass a larger dataset of variable length contractions. Of the 3 classifiers evaluated, both the LDA and MLP demonstrated higher but not significantly different ($p > 0.05$) classification accuracies than the SVM classifier—a result that may be influenced by our use of the default regularization, and gamma parameters for the RBF kernel of the SVM classifier that are used to balance a smooth decision boundary against classifying training points correctly [20][21]. Notwithstanding some fluctuations between individual classifier models, the relatively high accuracy performance shared across all classifiers demonstrates the feasibility of using MUAP features for motion classification as discussed in further detail below.

A. MUAP features amplify movement discriminability.

Despite a wide variety of classifier architectures and feature extraction techniques [9], existing motion classification algorithms continue to rely on time and frequency domain features based on the aggregate values of the raw sEMG signal. Given that the statistical distribution of amplitudes within the EMG signal is known to be non-uniform [22], aggregating windows of EMG data can both attenuate and suppresses high and low EMG amplitudes, limiting the dynamic range and expressiveness of aggregate measures as features for use in pattern recognition applications. In contrast, our targeted approach focuses on features within individual sEMG waveforms representing one or more superimposed MUAPs, mirroring the capability of EMG decomposition algorithms to separate the contribution of individual MUAPs and their superpositions from spurious features of noise and motion artifacts, while providing a wider dynamic range of signal amplitude and duration features. Our classification results outperform other state of the art real-time capable algorithms in [10] and [23] which only report accuracies at or below the 80th percentile. These results indicate that our use of MUAP features facilitate motion classification to more clearly discriminate signal patterns associated with different motions than can be gleaned from raw sEMG signal features alone.

B. MUAP features are feasible for accurate, real-time motion classification

We found that MUAP features—which need only be calculated on spliced waveforms of the sEMG signal—were computationally feasible of being tracked in real-time. This finding allowed our motion classifier algorithms to sustain real-time performance on relatively low-cost hardware (i.e., readily available CPUs and computer memory architectures), with an average processing time <40ms for each 100-ms window of data across all 3 classifiers tested. This stands in contrast to other computationally expensive approaches [24][11] which trade-off real-time performance for accuracy. While our algorithms also allow boosting performance via time-accuracy tradeoffs by increasing the window majority vote size, our pattern recognition algorithms maintain accuracies >90%, while operating well within the recommended maximum delay of 250ms for real-time pattern recognition systems [25] and offering a simple pathway to integrate with real-time prosthetic control systems – a focus of future work.

A. Multi-channel sensors enable MUAP-based motion classification.

A critical foundation of MUAP-based motion classification is the use of high resolution, multi-contact, multi-channel mini grid sensors. The use of these sensors allows for recording of sEMG from multiple (5mm spaced) adjacent vantage points on a muscle, which has the effect of increasing MUAP discriminability and feature dimensionality for our extraction and classification algorithms. This stands in contrast to other multi-sensor or high-density grid configurations whose monopolar configuration and large surface area can easily introduce noise and movement artifact distortions [26][27].

Our focus on mini-grid sensors has allowed us to achieve improved accuracies even when using just 4 specifically placed sensors, compared with commercial pattern recognition systems that employ at minimum 6-8 sensors [2]-[4] spaced circumferentially around the forearm or targeted muscles. This agrees with prior work [28] that showed that a smaller number of intelligently placed channels can maintain or even improve classification accuracy when compared to generic high-channel count sEMG grid sensors. Increasing the number of sensors would likely allow us to further increase accuracy by adding training data to discriminate motions with the greatest (3.1%) classification errors.

Study Limitations

Due to the COVID-19 pandemic, the research presented in this study was limited to healthy, intact humans. While our prior work [29] demonstrated the feasibility of real-time motor unit based neural interfaces for persons with limb-difference, future research should evaluate MUAP-based motion classification performance specific to the user populations and applications in rehabilitation and prosthetics.

V. Conclusion

In this work, we designed a real-time pattern recognition system for classifying motions of arm & hand. We tested these algorithms on 6 motions performed across a range of muscle contraction intensities by control participants with intact limbs (n=10) and achieved median classification accuracies ranging from 91.3% to 93.3% and an average processing time of approximately 40 ms across three different classifiers. These results highlight a critical attribute of motor unit based neural interfaces: motor unit features can provide

multi-DOF motion classification that is accurate, repeatable, and real-time capable. By leveraging features inherent to MUAP waveforms within the sEMG signal, motor unit based neural interfaces have the potential increase the DOF and functional control for its users and improve the performance of other pattern recognition approaches, supporting further development of our MU Drive neural interface system. Future research will refine and integrate MUAP-based motion classification with the proportional control demonstrated in our previous work to provide a comprehensive neural interface system that can be adapted to the control of prosthetic, computer, and robotic systems.

ACKNOWLEDGMENT

The authors are grateful to all participants participating in testing for their time and patience. Altec and Delsys Inc. are commercial entities involved in the research and manufacture of sensor technology for health and human performance.

REFERENCES

[1] B. Hudgins, P. Parker, R. N. Scott, A New Strategy for Multifunction Myoelectric Control. *IEEE Trans. Biomed. Eng*. 40, 82–94 (1993).

[2] Coapt LLC, https://www.coaptengineering.com/technology.html

[3] IBT LLC, SENSE https://www.i-biomed.com/sense.html (Accessed Mar, 2023)

[4] Ottobock SE, MYO PLUS https://www.ottobock.com/ (Accessed Mar, 2023)

[5] B. A. Lock, K. B. Englehart, and B. Hudgins, "Real-time myoelectric control in a virtual environment to relate usability vs. accuracy," in *Proc. 2005 MyoElectric Control. Prosthetics Symp*., pp. 17–20, 2005.

[6] A. Phinyomark, P. Phukpattaranont, and C. Limsakul, "Feature reduction and selection for EMG signal classification," *Expert Syst. Appl*., vol. 39, no. 8, pp. 7420–7431, Jun. 2012.

[7] R. Hu, X. Chen, X. Zhang, and X. Chen, ''Adaptive electrode calibration method based on muscle core activation regions and its application in myoelectric pattern recognition,'' *IEEE Trans. Neural Syst. Rehabil. Eng*., vol. 29, pp. 11–20, 2021.

[8] A. Fougner, E. Scheme, A. D. C. Chan, K. Englehart, and Ø. Stavdahl, ''Resolving the limb position effect in myoelectric pattern recognition,'' *IEEE Trans. Neural Syst. Rehabil. Eng*., vol. 19, no. 6, pp. 644–651, Dec. 2011

[9] N. V. Iqbal, K. Subramaniam, and S. Asmi P., "Robust feature sets for contraction level invariant control of upper limb myoelectric prosthesis," *Biomed. Signal Process. Control*, vol. 51, pp. 90–96, 2019.

[10] E. Campbell, A. Phinyomark, and E. J. Scheme, "Current Trends and Confounding Factors in Myoelectric Control: Limb Position and Contraction Intensity," *Sensors*, vol. 20, no. 6, p. 1613, 2020.

[11] Islam, M. J., Ahmad, S., Haque, F., Reaz, M. B. I., Bhuiyan, M. A., & Islam, M. R. (2021). A novel signal normalization approach to improve the force invariant myoelectric pattern recognition of transradial amputees. *IEEE Access, 9*, 79853-79868.

[12] Stachaczyk, M., Atashzar, S. F., Dupan, S., Vujaklija, I., & Farina, D. (2020). Toward universal neural interfaces for daily use: Decoding the neural drive to muscles generalises highly accurate finger task identification across humans. *Ieee Access, 8*, 149025-149035.

[13] J. C. Kline and C. J. De Luca, "Error reduction in EMG signal decomposition," *J. Neurophysiol*., vol. 112, no. 11, pp. 2718–2728, Dec. 2014.

[14] C. J. De Luca, S.-S. Chang, S. H. Roy, J. C. Kline, and S. H. Nawab, "Decomposition of surface EMG signals from cyclic dynamic contractions," *J. Neurophysiol*., vol. 113, no. 6, pp. 1941–1951, Mar. 2015.

[15] D. Pereira Botelho, K. Curran, and M. M. Lowery, "Anatomically accurate model of EMG during index finger flexion and abduction derived from diffusion tensor imaging," *PLOS Comput. Biol*., vol. 15, no. 8, p. e1007267, 2019.

[16] T. Hoshizaki, E. A. Clancy, D. A. Gabriel, and L. A. Green, "The reliability of surface EMG derived motor unit variables," *J. Electromyogr. Kinesiol*., vol. 52, p. 102419, Jun. 2020.

[17] C. J. De Luca, "The use of surface electromyography in biomechanics," *J. Appl. Biomechan*., vol. 13, pp. 135–163, 1997.

[18] Kramer, Oliver, and Oliver Kramer. "Scikit-learn." Machine learning for evolution strategies (2016): 45-53.

[19] Lam, Siu Kwan, Antoine Pitrou, and Stanley Seibert. "Numba: A llvm-based python jit compiler." In *Proceedings of the Second Workshop on the LLVM Compiler Infrastructure in HPC*. 2015.

[20] F. Pedregosa, G. Varoquaux, A. Gramfort, V. Michel, B. Thirion, O. Grisel, Machine Learning in Python. *J. Mach. Learn. Res*. 12, 2825–2830 (2011).

[21] E. J. Scheme, K. B. Englehart, Training Strategies for Mitigating the Effect of Proportional Control on Classification in Pattern Recognition Based Myoelectric Control. *J. Prosthet. Orthot*. 25, 76–83 (2013).

[22] Nazarpour, Kianoush, et al. "A note on the probability distribution function of the surface electromyogram signal." *Brain research bulletin* 90 (2013): 88-91.

[23] Khushaba, Rami N., et al. "A long short-term recurrent spatial-temporal fusion for myoelectric pattern recognition." *Expert Systems with Applications* 178 (2021): 114977.

[24] S. Hua, C. Wang, Z. Xie, and X. Wu, ''A force levels and gestures integrated multi-task strategy for neural decoding,'' *Complex Intell. Syst*., vol. 6, no. 3, pp. 469–478, Oct. 2020.

[25] Smith, L. H., Hargrove, L. J., Lock, B. A., & Kuiken, T. A. (2010). Determining the optimal window length for pattern recognition-based myoelectric control: balancing the competing effects of classification error and controller delay. *IEEE transactions on neural systems and rehabilitation engineering*, 19(2), 186-192.

[26] Stachaczyk, Martyna, S. Farokh Atashzar, and Dario Farina. "Adaptive spatial filtering of high-density EMG for reducing the influence of noise and artefacts in myoelectric control." *IEEE Transactions on Neural Systems and Rehabilitation Engineering* 28.7 (2020): 1511-1517.

[27] Lee, Jin, Alexander Adam, and Carlo J. De Luca. "A simulation study for a surface EMG sensor that detects distinguishable motor unit action potentials." *Journal of neuroscience methods* 168.1 (2008): 54-63.

[28] Huang, H., Zhou, P., Li, G., & Kuiken, T. A. (2008). An analysis of EMG electrode configuration for targeted muscle reinnervation based neural machine interface. *IEEE Transactions on Neural Systems and Rehabilitation Engineering*, 16(1), 37-45.

[29] M. D. Twardowski, S. H. Roy, Z. Li, P. Contessa, G. De Luca, J. C. Kline, Motor unit drive: a neural interface for real-time upper limb prosthetic control. *J. Neural Eng*. 16, 016012 (2019).